Integrative Biology, 2019, 00(00), 1–13

doi: 10.1093/intbio/zyz018
Original Article

ORIGINAL ARTICLE

Ranking migration cue contributions to guiding individual fibroblasts faced with a directional decision in simple microfluidic bifurcations

Quang Long Pham[1,†], Anh Tong[1,†], Lydia N. Rodrigues[1], Yang Zhao[1], Migle Surblyte[2], Diomar Ramos[1], John Brito[1], Adwik Rahematpura[1], and Roman S. Voronov[1,*]

[1]Otto H. York Department of Chemical and Materials Engineering, New Jersey Institute of Technology, Newark, NJ, USA and [2]Ying Wu College of Computing Sciences, Department of Computer Science, New Jersey Institute of Technology, Newark, NJ 07102, USA

*Corresponding author. E-mail: rvoronov@njit.edu

Abstract

Directed cell migration in complex micro-environments, such as in vivo pores, is important for predicting locations of artificial tissue growth and optimizing scaffold architectures. Yet, the directional decisions of cells facing multiple physiochemical cues have not been characterized. Hence, we aim to provide a ranking of the relative importance of the following cues to the decision-making of individual fibroblast cells: chemoattractant concentration gradient, channel width, mitosis, and contact-guidance. In this study, bifurcated micro-channels with branches of different widths were created. Fibroblasts were then allowed to travel across these geometries by following a gradient of platelet-derived growth factor-BB (PDGF-BB) established inside the channels. Subsequently, a combination of statistical analysis and image-based diffusion modeling was used to report how the presence of multiple complex migration cues, including cell-cell influences, affect the fibroblast decision-making. It was found that the cells prefer wider channels over a higher chemoattractant gradient when choosing between *asymmetric* bifurcated branches. Only when the branches were *symmetric* in width did the gradient become predominant in directing which path the cell will take. Furthermore, when *both* the gradient and the channels were *symmetric*, contact guidance became important for guiding the cells in making directional choices. Based on these results we were able to rank these directional cues from most influential to the least as follows: mitosis > channel width asymmetry > chemoattractant gradient difference > and contact-guidance. It is expected that these results will benefit the fields of regenerative medicine, wound healing and developmental biology.

Insight, innovation, integration

Cells making directional decisions, while navigating the micro-confines of tissue pores, are commonly faced with a combination of chemical and physical cues. For the first time, we rank relative importance of these physiologically

(*Continued*)

[†]The first two authors contributed equally to the manuscript.

Received October 16, 2018; **revised** April 4, 2019; **editorial decision** May 20, 2019; **accepted** May 21, 2019

STANDARD

(Continued)

significant stimuli, from most influential to least as follows: mitosis, physical micro-confinement, mild chemoattractant gradient, and contact-guidance. Furthermore, we integrated a novel image-based modeling approach with simple microfluidic bifurcation experiments, in order to assess the localized chemoattractant consumption by the individual cells. These results and the hybrid method have potentially widespread implications to the fields of wound healing, developmental biology, and regenerative medicine.

INTRODUCTION

Directional decision-making during cell migration is important for regenerative medicine (e.g., tissue engineering and wound healing) [1] and developmental biology [2, 3], since tissue development depends on how the cells distribute themselves within the complex pores of the extra-cellular matrix [3–5]. However, forecasting cell migration through microscopic pores is challenging because their directional decisions are affected by a *combination* of different factors: such as, physical confinement [6–10], varying levels of biochemical agonist gradients [11, 12], mitosis [13], and contact guidance [10]. Therefore, the interplay between these factors is crucial to unraveling the underlying biology mechanisms behind the migration directionality and consequently, to achieving control over cell behavior.

Here, we are specifically interested in the behavior of fibroblasts, which play a vital role in tissue formation: such as synthesizing, remodeling, and depositing extracellular matrix materials [14]. This cell type is known to migrate as individual cells (as opposed to collective migration), when squeezing through the microscopic tissue pores [15]. Typically, single cell migration studies induce chemotaxis by establishing stable chemoattractant gradients within the confines of microfluidic assay pores [9, 10, 16–19]. Such studies tend to quantify the directional decisions (i.e., a choice of whether to go left or right) of the migrating cells as a function of isolated factors (e.g., channel length, width, concentration gradient, contact guidance, etc.). At most two of the migration cues are explored at a time [20]. Yet, the cells encounter multiple simultaneous cues when navigating tissue pores in vivo. Hence, it is imperative to have a model that better describes the combinatorial effects of numerous cues on the cells' directional decisions (i.e., where a single choice must be selected from multiple possible paths).

Furthermore, conventional migration studies typically do not consider the effects that single cells have on each other's directional-decision making. Yet, we recently demonstrated that fibroblasts migrating through a microfluidic maze, consisting of two uneven through-paths, tend to affect the directional decisions of the cells trailing behind them [18]. Specifically, it was found that when a leading cell takes a shorter path, its follower is likelier to take a longer path, and vice versa. Furthermore, we used image-based simulation to show that this happens due to localized consumption of the chemoattractant by the individual cells, which in turn modifies the direction of the steepest gradient increase for their neighbors. Since this finding is in contradiction to what would be expected from classical chemotaxis theory (i.e., from the global chemoattractant gradient established in the maze), cell-cell influences should also be taken into account when ranking the relative importance of the directional cues to the migratory decisions.

In order to address these gaps in knowledge, while taking into account the cell-cell influences on each other, here we use a migration model which consists of bifurcated microfluidic channels of varying widths. A gradient of platelet-derived growth factor-BB (PDGF-BB) is used to induce migration of normal human dermal fibroblasts (NHDF) into the channels [21, 22]. The PDGF-BB is a fibroblasts 'mitoattractant' (i.e., both a chemoattractant [23–25] and a mitogen [26–29] at the same time). Hence, when the cells reach the bifurcation, they are exposed to simultaneous external cues, including: chemoattractant gradient differences, channel width bias, contact guidance, and cell-cell influences (e.g., localized consumption of PDGF-BB and mitosis). The gradient changes caused by the cell endocytosis are calculated using the same image-based modeling approach as in our prior work [18, 30]. With this framework in place, we compare the relative importance of the multiple directional cues and, for the first time, rank them based on their individual contributions to inducing and guiding the cell migration in micro-confined pores. Furthermore, we demonstrate that the results hold for multiple cell types by presenting the same study, but repeated with mouse embryonic (NIH/3T3) fibroblasts (see Supplemental Materials).

METHODS

Materials

Polydimethylsiloxane (PDMS) Sylgard 184 was purchased from Dow Corning (Midland, MI). Negative photoresist SU-8 was purchased from Microchem (Newton, MA). Bovine collagen Type I 3 mg ml^{-1} solution (PureCol) was purchased from Advanced Biomatrix (San Diego, CA). Recombinant rat platelet-derived growth factor-BB (PDGF-BB) was purchased from R&D Systems (Minneapolis, MN) and human-derived from VWR (Radnor, PA). Culture media was prepared from Minimum Essential Medium (MEM) (Sigma, MO) supplemented with 10% (v/v) fetal bovine serum (FBS) (VWR, Radnor, PA) and 1% (v/v) penicillin-streptomycin (10 000 U mL^{-1}) (Thermofisher, Waltham, MA). Basal media was composed of MEM supplemented with 1% (v/v) penicillin-streptomycin. For incubation in 5% CO_2 atmosphere, media was buffered by 26 mM sodium bicarbonate (Sigma, MO). CO_2-independent media buffered by 20 mM HEPES (Sigma, MO) was used for the microscope stage-top experiment.

Device concept

The PDMS device was made from PDMS and consisted of an array of 32 microfluidic 'maze' channels, all of which were 20-μm high. The channels connected a central chemoattractant (i.e., PDGF-BB) reservoir to a cell seeding area surrounding the device (see Fig. 1-**LEFT**). Each maze consisted of two 15-μm-wide 'common' (i.e., that all cells had to pass through) channels; one 'feeder' and one 'exit' (see Fig. 1-**RIGHT**). The feeder channel was bifurcated into two 'branched' channels of the same length but varying widths – ranging from 15 to 75 μm. The two branches merged at the second bifurcation, which led to the 15-μm wide 'exit' channel. With this setup, the cells were allowed to migrate from the seeding area towards the central

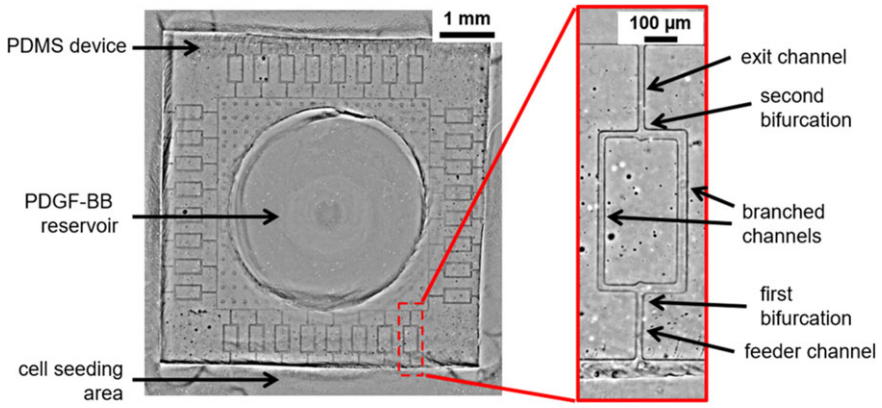

Figure 1. Phase-contrast microscopy showing the device concept: LEFT - 32 'mazes' surrounding a central chemoattractant reservoir; RIGHT - Inset is a magnified view of a single 'maze' with the different types of channels labeled.

reservoir, following a chemoattractant concentration gradient established inside of the maze channels.

Device fabrication

The masks for the devices were sketched using AutoCAD (Autodesk, Mill Valey, CA) and printed at 50 800 DPI on a transparency (Fineline Imaging, Colorado Springs, CO). The devices were created using replica molding technique and the master mold was fabricated from SU-8 negative photoresist using soft photolithography technique and the custom-built mask aligner, both of which are described in our prior publication [31]. The SU-8 2010 photoresist was spin-coated at 2000 rpm on a 4-in Silicon wafer, exposed to UV light, and developed to yield 20-μm-tall microfluidic channels. The internal surfaces of the microfluidic channels were treated with Collagen Type I (150 μg ml^{-1} coating concentration) overnight (≥ 12 hours) at 4°C or incubated at least 3 hours at 37°C.

Cell preparation

Mouse embryo NIH/3T3 (ATCC® CRL-1658™) fibroblasts and normal human dermal fibroblasts (NHDF) (ATCC® PCS-201–012™) were purchased from ATCC (Manassas, VA). Prior to being transferred to the microfluidic device for the migration experiments, the cells were incubated in the culture media inside of T75 flasks. The flasks were kept at 37°C and in a humidified atmosphere of 5% CO_2 in air. The culture media was changed every two days to ensure normal cell growth. Prior to the migration experiments, the cells were trypsinized from the T75 flasks and loaded into the chip. A seeding density of about 50 000 cells cm^{-2} was used. The chip was incubated at 37°C under 5% CO_2 for 6 hours to allow for the cell-surface adhesion. Then the NIH/3T3 cells were cultured in serum-starved media (MEM supplemented with 1% penicillin-streptomycin) for 6 hours, while the NHDF culture media was supplemented with 0.5% FBS to provide minimal survival condition for the long-term experiments (because they are slower).

Cell migration experiment

For full details of the experimental setup, see our previously published work [18]. Briefly, at the start of the experiment, cell culture media in the chip was replaced with CO_2-independent media (basal for NIH/3T3 or 0.5% FBS for NHDF), buffered by HEPES and supplemented with 1% penicillin-streptomycin. 20 μL of the basal media supplemented with 50 ng mL^{-1} PDGF-BB was then added into the central reservoir of each device. Typically, the device was mounted on a condition chamber which is equipped with a temperature regulation system and a humidified environment. Time-lapse phase-contrast imaging of the fibroblast migration was performed using a fully automated Olympus IX83 microscope fitted with a 10X phase-contrast objective (Olympus, Japan), a CMOS camera (Orca Flash 4.0 V2, Hamamatsu, Japan), and an autofocus module (ZDC, Olympus, Japan). Time-lapse images were automatically captured at a 27 minute interval for duration of 5–10 days (media refreshed after 5 days) for NHDF and at a 15 minute interval for a duration of 24 hours for NIH/3T3 cell. For each device at each time step, 36 tile images were acquired at different locations, stitched, and stabilized using an in-house Matlab® 2016b code (MathWorks, Inc., Natick, MA).

Data analysis

The migrating cells were tracked using the Manual Tracking plug-in for ImageJ software (National Institutes of Health) [32]. The directional decisions chosen by each individual cell at the bifurcation were determined via manual observation. Quantitative data of cell sequences was generated using an in-house Matlab® 2016b code (MathWorks, Inc., Natick, MA). Significance level was determined by using a non-parametric test for a binomial distribution, unless otherwise stated. Statistical significance was set as $p < 0.05$.

Simulation of transient PDGF-BB gradient in the presence of migrating cells

For a complete description of the model see our previously published paper [18]. The PDGF-BB concentration gradient established between the two ends of the maze was simulated numerically using COMSOL 5.3a Multiphysics (COMSOL, Burlington, MA). Constant concentration boundary conditions, corresponding to the experiment, were set to $C_{P,exit} = 50$ ng mL^{-1} PDGF-BB at the maze exit and zero at the maze entrance. A diffusion coefficient of $D_{P,maze} = 1 \times 10^{-10}$ m^2 s^{-1} was used to represent the PDGF-BB (MW = 25 kDa) in an aqueous solution [33]. Chemoattractant gradient values at every point in the maze were calculated from the vector magnitude of two components, x-axis (horizontal) and y-axis (vertical), both of which increased towards the higher concentration of PDGF-BB.

Phase-contrast microscopy time-lapse images were used to incorporate the effects of the presence of the cells into the COMSOL simulations. While the maze geometry remained static, the cell shapes and locations were obtained via image processing and passed into the diffusion solver. The cell migration was updated at intervals of $\Delta t = 15$ min (corresponding to the experimental acquisition times). Both the natural decay of PDGF-BB and its depletion via endocytosis by fibroblasts were taken into account. These effects were represented by a decay constant $k_{decay} = 2.78 \times 10^{-5}\ s^{-1}$ and an endocytosis rate constant $k_{endocytosis} = 0.555\ cm^3\ g^{-1}\ s^{-1}$, respectively [34, 35]. Hence, the following consumption terms were added to the COMSOL model: $-k_{decay}\ C_P$ everywhere in the maze and $-k_{endocytosis}\ C_f\ C_P$ in the cell domains. Here, 'k' represents reaction rate constants, C_P is the local concentration of PDGF-BB and C_f is the fibroblast 'density' – an analog of a chemical species concentration in a continuum representation of the cells. However, since our model had discrete cells, we assumed that $C_f = C_{f,max} = 0.1\ g\ cm^{-3}$ (corresponding to $\bar{f}$ in Menon *et al.*), which was derived based on the carrying capacity of the fibroblast cells. Moreover, the diffusivity of the PDGF *inside* of the cells $D_{P,cell}$ was arbitrarily set to two orders of magnitude slower than in the channels, or $10^{-12}\ m^2\ s^{-1}$, in order to simulate the effect of the chemoattractant diffusion being obstructed by the cells.

RESULTS

In this paper, we set out to compare (and rank) the relative contributions that different physiochemical stimuli have on the directional decisions made by single cells migrating in the confinement of microscopic pores. Among the studied effects are mitosis, channel geometry differences, localized chemoattractant gradient changes and contact guidance – all of which are encountered by the cells traversing tissue pores in vivo. Given that prior studies only considered directional decision-making in microfluidic channels of identical width, we first wanted to assess how the process is affected by asymmetric confinement. To do that, migration of fibroblasts was induced inside of simple microfluidic 'mazes' consisting of bifurcating channels of identical lengths, but with a different branch width ratio (BWR).

Experimental observations show strong preference for wider branches and a weak dependence on cell sequence

Specifically, the left branch of the bifurcation was always kept 15 μm wide while the width of the right branch was varied as follows: 15 μm (i.e., 1X BWR), 22.5 μm (i.e., 1.5X BWR), and 45 μm (i.e., 3X BWR). This is shown in Fig. 2a.

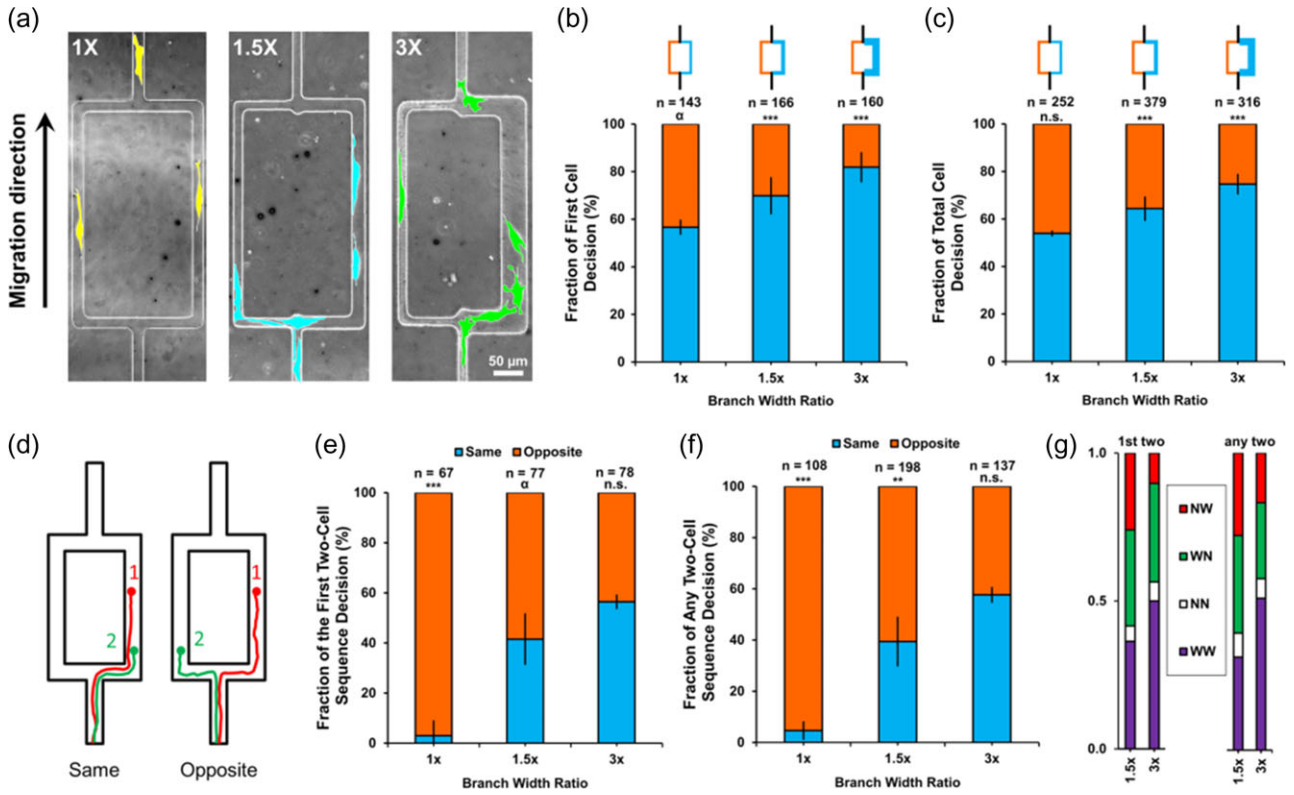

Figure 2. NHDF directional decision-making statistics when faced with a choice between asymmetric branch widths. (a) Phase contrast microscopy images of cells migrating in mazes showing the three different branch arrangements explored in this study: 1X, 1.5X and 3X. Cells are false-colored for increased visibility. (b) Fraction of the decision bias made only by the 1st cells to encounter the bifurcation, as a function of BWR. (c) Fraction of the decision bias made by any individual cells to enter the maze. (d) Graphic illustrating the definition of the 'same' and 'opposite' directional decision sequences made by two consecutive cells. (e) Fraction of the decision sequences made by only the first two cells to encounter the bifurcation. (f) Fraction of the decision sequences made by any two consecutive cells to encounter the bifurcation. (g) Fraction of decision sequences made by the first two cells and by any two consecutive cells with respect to the BWR. WW: both the leading and the follower cells select the wider branch; NN: both cells select the narrower branch; WN: the leading cells select the wider branch while the trailing cells select the narrower branch; NW: the leading cells select the narrower branch while the follower cells select the wider branch. In (b),(c): 'n' indicates the number of cells making a decision; in (e), (f): 'n' is the total number of sequences; 'n.s.' is not statistically significant. α: $p < 0.1$; *: $p < 0.05$; **: $p < 0.01$; ***: $p < 0.001$.

Initially, we quantified the cell decision-making at the first bifurcation, which is closest to the maze entrance. In Fig. 2b, the 1st cells to encounter the bifurcation displayed no obvious preference between the two branches of the identical widths ($p > 0.05$). On the other hand, a significant bias towards the wider branch was observed when there was a width difference between the two bifurcation branches. In fact, Fig. 2b shows that the larger the BWR, the higher the bias towards the wider channel. This is evidenced by the trend in the bias confidence level, which for NHDF cells equals to $p = 1.6\times10^{-7}$ for 1.5X BWR and 5.5×10^{-17} for 3X BWR. Furthermore, the same trend still holds true even when *all* individual cells to enter the maze are considered, not just the first two (see Fig. 2c). Overall, the results shown in Fig. 2b–c suggest that a wider, open space is more attractive to the migrating fibroblasts than the confinement of the symmetric 1X BWR.

Next, we assessed whether cell-cell effects play a role in the fibroblast directional decision-making. This is done by accounting for the cell *sequences* when analyzing the bifurcation branch choices. For clarity, when *both* the leading and the trailing cells commit to the same path, this is referred to as the 'same' sequence; while the case when the cells make *different* choices from each other is termed as 'opposite' sequence. This notation is illustrated in Fig. 2d.

Like in Fig. 2b, we initially considered the decisions made only by the first two cells to encounter the bifurcation. From this analysis, it was observed that as the difference in the branch widths increased, the first two cells had a higher tendency of making the same choice (see Fig. 2e). The same trend persisted when the sequences made by any two consecutive cells were considered (see Fig. 2f). And like in Fig. 2c, the fibroblasts' choices were biased towards the wider branches. For example, the wide-wide decision sequence accounted for roughly half of the decisions made in the 3X BWR maze (see Fig. 2g).

Finally, **Supplementary Figure 1** shows that the NIH/3T3 results are in agreement with the NHDF trends presented in this section.

Image-based modeling of the localized chemo-attractant gradient in the bifurcated mazes

Next, we wanted to explain the observed experimental behavior via computational image-based modeling. In our prior work, the decision-making of fibroblasts during chemotaxis in micro-confined environments was found to be largely influenced by the changes in localized concentration gradients of PDGF-BB [18]. Specifically, the fibroblasts were found to influence each other's decisions via PDGF-BB consumption (i.e., endocytosis) and via blockage of its transport in the confined channel space. Hence, we applied the same image-based modeling approach to the three different channel-width biases mentioned above: namely, 1X, 1.5X and 3X BWR. The simulation results for this are shown in Fig. 3.

Fibroblasts' preference for the wider branches is not dictated by the PDGF-BB gradient

From Fig. 3, it is evident that the 1st cells to encounter the bifurcation experience no discrepancy in the gradient between the two branches, regardless of their width. However, as mentioned previously, the fibroblasts do tend to prefer the wider branches with a high probability. Hence, this preference appears to not be influenced by the PDGF-BB gradient (at least not in the case of the 1st cells). Additionally, there was also a trend in the average

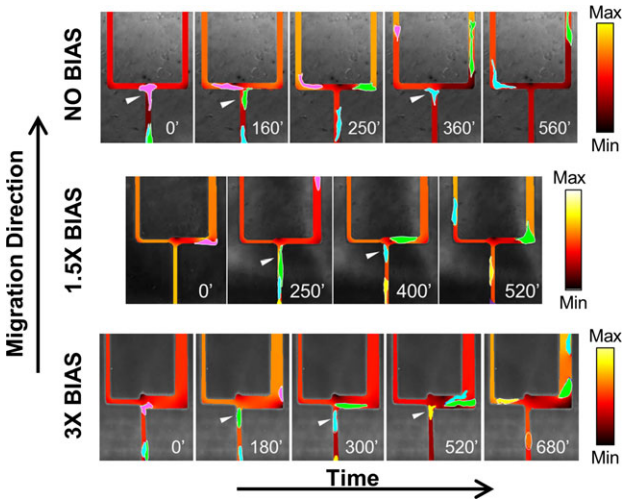

Figure 3. Image-based simulation of localized PDGF-BB gradient modifications caused by fibroblasts traveling inside of different BWR bifurcations. TOP: time montage showing the gradient dynamics inside of a symmetric 1X BWR bifurcation. MIDDLE: time montage showing the gradient dynamics inside of an asymmetric 1.5X BWR bifurcation. BOTTOM: time montage showing the gradient dynamics inside of an asymmetric 3X BWR bifurcation. White arrows indicate the cells that are about to make a directional choice. Cells are false colored for visibility and their order is color-coded as follows: magenta – 1st cell, green – 2nd cell, cyan – 3rd cell, yellow – 4th cell, etc. Max corresponds to a gradient value of 1×10^{-3} mol/m^4.

decision time for these cells. Specifically, it took NHDF cells 247 ± 21 min ($n = 64$), 177 ± 18 min ($n = 81$), and 169 ± 12 min ($n = 97$) to commit to a branch for the 1X, 1.5X and the 3X BWR cases, respectively. Similarly, it took NIH/3T3 cells 172 ± 122 min ($n = 27$), 122 ± 81 min ($n = 17$), and 109 ± 60 min ($n = 27$) to commit to a branch for the 1X, 1.5X and the 3X BWR cases, respectively. In other words, the fibroblasts decide which way to go *faster* when there is a higher disparity in the width between the two branch choices. This makes sense, given that the larger the width, the stronger the directional cue of the wide branch appears to motivate the fibroblasts. Furthermore, longer decision times are expected for the 1st cells to face the symmetrical bifurcations, because they may need to do a more thorough evaluation of which direction is preferable. Given all things being equal, their decision is ultimately prone to random selection rather than being guided by any directional cues.

Trailing cells alternate paths less in asymmetric mazes than in symmetric ones

When sequence order is taken into account, however, the trailing cells are expected to see a significantly lower PDGF-BB gradient in the branches chosen by the leaders. This is due to the consumption of the chemoattractant and the obstruction of its transport in the narrow branches. Therefore, the 2nd cells should have a higher tendency of selecting the opposite path, instead of trailing the 1st cells. As expected, Fig. 3-TOP pane shows that this holds true for the *symmetric* bifurcations (see Video 1): the 2nd cells to encounter them take the *opposite* path at a high frequency of 97.01 ± 6.13% ($p = 1.5\times10^{-7}$) for NHDF and 89.5 ± 2.5% ($p = 8\times10^{-6}$) for NIH/3T3. However, in the case of the *asymmetric* 1.5X and 3X BWR, there is a higher number of the 2nd cells taking the *same* path as the 1st ones for both types of fibroblasts (see Video 2 and 3, respectively). This could be explained by the diffusion of the chemoattractant being less limited in the wider branches, since the chemical can go around the leading

cells easier. Therefore, the gradient differences between the two branches are less obvious to the trailing cells in the asymmetric bifurcations (see 250' and 180', Fig. 3-MIDDLE and BOTTOM panes, respectively) than in the symmetric ones (see 160', Fig. 3-TOP pane). Consequently, the availability of a wider space for migration outweighs the minute differences in the chemoattractant gradient for these cells.

Sufficient fibroblast crowding outweighs the desire to migrate into wider channels

Similar to the first two cells in the *symmetric* bifurcation, the 3rd and 4th cells to enter follow the alternating decision-making pattern, which is driven by the steeper gradient (see 360', Fig. 3-TOP pane). In the *asymmetric* cases however, the behavior varies depending on the accumulation of cells in the wider branches. For example, a 3rd cell in the 1.5X bifurcation (see 400', Fig. 3-MIDDLE pane is faced with a *significantly* (approximately an order of magnitude) *lower* gradient inside the wider branch when compared to the narrower one. This is due to the presence of both the 1st and the 2nd cells in the wider branch at the same time. Together, the two cells both consume and/or block the PDGF-BB so much, that the 3rd cell behind them opts to migrate into the narrower path (despite it being less desirable). A similar situation occurs in the 3X bifurcation, where the simultaneous presence of the 2nd and 3rd cells in the wider branch (see 520', Fig. 3-BOTTOM pane) ultimately diverts the 4th cell into the narrower, less-desirable route (680', Fig. 3-BOTTOM pane). Hence, there appears to be a combination of PDGF-BB consumption and obstruction that causes that the cells to consider the path unacceptable and go into the narrower path instead.

In summary, this section showed that the difference in the gradient steepness has a smaller influence on the fibroblast directional decision-making process than does the BWR. Hence, it may be concluded that the chemoattractant gradient is *secondary* to the branch width effect, when it comes to influencing the directionality of fibroblast migration.

Control experiments prove that branch symmetry (not width alone) causes decision alternation

Thus far, we have demonstrated that the sequence-dependent alternation occurs less frequently when the width asymmetry between the two bifurcation branches becomes higher. However, it is also possible that the wide size of the branch (not the asymmetry) is responsible for the observed migration behavior. Hence, we performed a control experiment where the cells were allowed to migrate through *symmetric* bifurcation mazes with varying branch widths (see Fig. 4a). Similarly to the previous sections, we quantified the directional decision statistics of individual cells in two ways: 1) irrespective of their

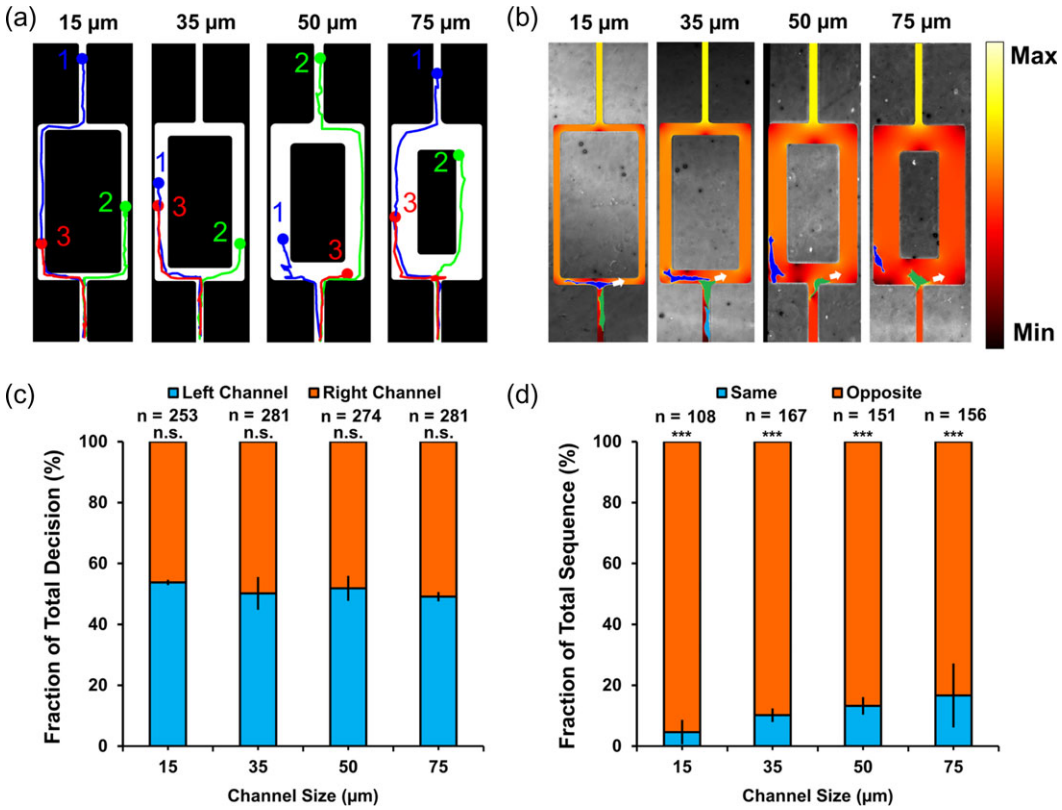

Figure 4. NHDF cells alternate directional decisions when faced with *symmetric* bifurcations. (a) Cell migration tracking line showing alternation patterns between consecutive cells. The lines are color-coded and numbered to indicate the order in which the cells make decisions at the bifurcation. Max corresponds to a gradient value of 1×10^{-3} mol/m^4. (b) Image-based simulation of the PDGF-BB gradient formed inside the symmetric bifurcation maze in the presence of migrating cells. Cells are false colored to increase the visibility. Blue cells are the leading cells while the green cells are the trailing ones. White arrows indicate the direction the green cells are about to take. (c) Fraction of *all* cells moving into one branch of the bifurcation versus the other, with respect to different branch widths. 'n' is the total number of cells making the decision. (d) Fraction of decisions made any two *consecutive* cells. 'Same' means that two consecutive cells took the same path – either left or right; while 'opposite' means that either the trailing cell turned left after the leading cells went into the right branch, or vice versa. 'n' is the total number of sequence events; 'n.s.': not statistically significant ($p > 0.1$); ***$p < 10^{-18}$.

sequence, and 2) with accounting for the sequences made by any two consecutive cells.

As expected, we observed that the cells display the alternating decision pattern regardless of the branch width, even though the difference in the gradient between the left and the right path is effectively negligible for all maze sizes (see Fig. 4b). Case in point are the wider branch sizes (e.g., 50 and 75 μm), which caused deviations from the alternation effects observed in the similar-sized *asymmetric* bifurcations. Yet, when the bifurcations are *symmetric*, the wider branches still experience alternation: for example, the fraction of the total decisions made by all individual cells, irrespective of their sequence, showed no significant preference for either branch (see Fig. 4c). Furthermore, the alternating sequences (a.k.a. 'opposite' path choices) dominated the fibroblast decision-making with a high statistical significance, regardless of the branch width (see Fig. 4d). The only exception is a slight decrease in the path alternation with a higher BWR. This is likely due to the localized gradient changes, caused by endocytosis of the preceding cell, becoming less apparent, as more of the chemoattractant passes through the wider channels.

Thus, these results suggest that the branch alternation is natural to all *symmetric* bifurcations; and that the minute chemoattractant gradient differences are the main factors, which drive the *trailing* cells toward the branches opposite from their *predecessors*. Finally, **Supplementary Figure 2** shows that the NIH/3T3 results are in agreement with the NHDF trends presented in this section.

Contact-guidance is key to directional decision-making when the leader cells are faced with symmetric choices

This section investigates the mechanism by which the 1st cells to enter the bifurcation of *symmetric* branch widths decide to commit to either one path or the other. Given that the chemoattractant gradient in both branches is the same, it is important to understand whether the cell decisions are merely random or are being driven by an unknown directional cue that needs to be elucidated. Interestingly, we noticed that in such *symmetrical* situations, the side of the feeder channel that the cell happens to be crawling along (a.k.a. being 'in contact' with) is important to its directional decision-making. Specifically, there are two scenarios that can occur when the cells are in contact with a wall: 1) they can either migrate into the branch of the same side as the contacted wall (a.k.a. 'contact-guided', Fig. 5a-LEFT), or 2) they can cross the feeder channel to the opposite side's branch (a.k.a. 'counter contact-guided', Fig. 5a-RIGHT). In either case, the gradient in both of the bifurcation branches is the same at the time when the decision is made.

According to Fig. 5b, roughly 90% of the NHDF cells display wall contact, while 10% do not. Among the former, ~75% commit to the same branch as the wall that they were touching,

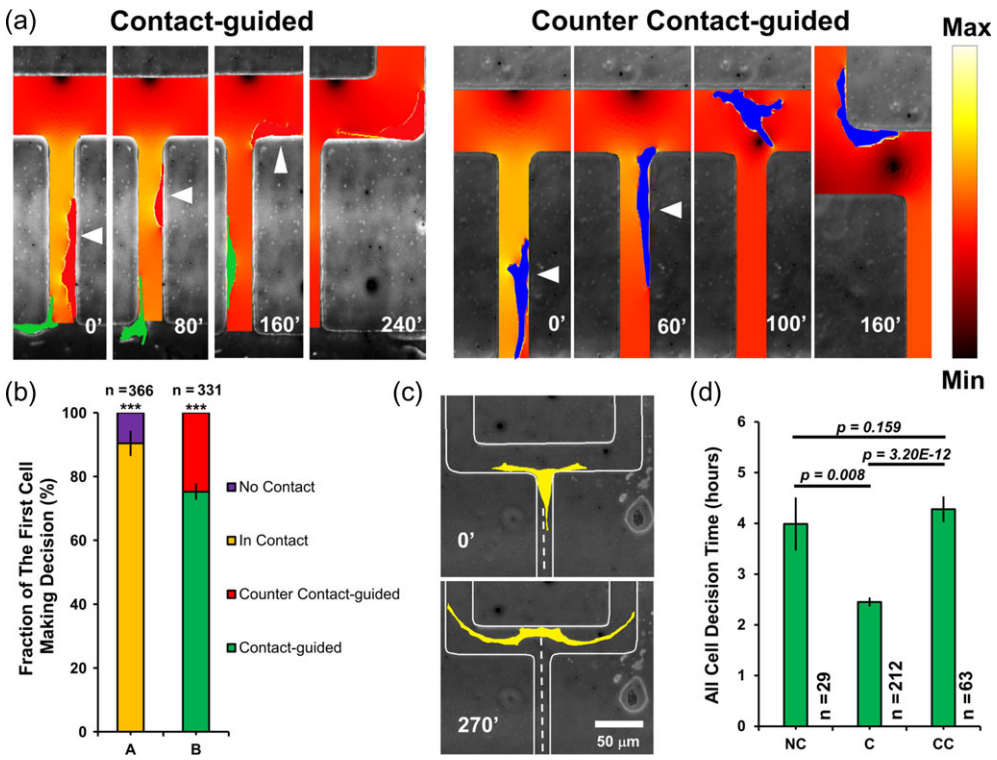

Figure 5. Contact-guidance is the prevalent cue in case of leader NHDF cells faced with width- and gradient- symmetric decisions. (a) Image-based simulation of PDGF-BB gradient showing two different scenarios of the cell contacting the wall of the feeder channel when reaching the first symmetric bifurcation. Cells can either select their path by following the wall that they are touching (i.e., contact-guided, LEFT) or go across to the opposite side of the channel (i.e., counter contact-guided, RIGHT). White arrows indicate cells being in contact. Cells are false-colored to increase the visibility. Max corresponds to a gradient value of 1×10^{-3} mol/m^4. (b) Fraction of 'In contact' versus 'No contact' when the 1st *cell* travels through the first bifurcation (bar A) and the fraction of it being contact-guided (bar B). Cells touching both walls are lumped into the 'no contact' group; 'n' indicates the number of cells; ***$p < 10^{-20}$. (c) Phase contrast microscopy montage showing the morphology of a cell touching both walls, thus not being contact-guided. The cell is false-colored yellow to increase visibility. (d) Decision time of the cells for the different contact guidance categories. Namely, NC (no contact), C (contact-guided), and CC (counter contact-guided). The statistical significance p-value between the mean of any two independent groups is tested using the nonparametric Mann Whitney U test [36] with a statistical significance level of 0.05. Values that laid more than three scaled median absolute deviations away from the median were considered to be outliers, and were removed using Matlab®.

while only ~25% move to the opposite branch. Furthermore, the cells that are contact-guided display a faster decision speed when compared to those that choose the counter contact-direction, and to those categorized as 'no contact' (including the cells touching both walls simultaneously). The latter cells are commonly seen to exhibit the extended body morphology shown in Fig. 5c. Since such membrane protrusions are a part of the spatial gradient-sensing mechanism of the migrating cells [37–39], the symmetric body extensions shown in Fig. 5c indicate that the cell is still in the process of determining the branch with the most attractive PDGF-BB gradient (which appears to be highly balanced at that time). The decision time is therefore prolonged extensively, and may take over 4 hours ± 31 minutes for the cell to make a commitment (Fig. 5d). Similarly the *counter* contact-guided cells take around 4 hours ± 15 minutes during the directional decision making process. On the contrary, the decision time of the cells being *contact-guided* is significantly faster: as short as 2 hours ± 5 minutes.

Overall, this section shows that the contact guidance is important for both the path selection and for the decision-making speed, given that everything else is equal. Thus, it is an imperative piece of information for forecasting the cell chemotaxis in *symmetric* microenvironments. Finally, **Supplementary Figure 3** shows that the NIH/3T3 results are in agreement with the NHDF trends presented in this section (with only a minor difference that the NIH/3T3 cells displayed less overall wall contact).

Contact-guidance is secondary to the chemoattractant gradient for trailing cells

In the previous section, the contact-guidance has been demonstrated to effectively drive the *leading* cells' directional decisions in *symmetric* gradient conditions. However, whether it is sufficiently strong to do the same in *asymmetric* gradient situations needs to be assessed. To that end, we characterized the decision-making of the *follower* cells to arrive at the bifurcation (while in contact with a wall) after the leading cells have already made their choice. In this case, there are essentially two possibilities: 1) the follower cells are *initially* either in contact with the same side of the feeder channel as the branch selected by the leading cells, or 2) they crawl along the opposite wall. Subsequently to each scenario, the follower cells can either follow the leading cells into their branch or choose the opposite branch (Fig. 6a). Therefore, the follower cells experience more degrees of freedom (i.e., there are more variables affecting their decisions) when compared to the leading cells.

We observed that more than 85% of the follower cells are *initially* in contact with a wall of the feeder channel and over 65% of those adhere to the side of the channel opposite to the branch chosen by the leading cells (Fig. 6b). Moreover, more than 75% of the follower cells that initially contacted the same side as the leading cell's branch selected the *opposite* branch. Interestingly, over 90% of the follower cells that initially contacted the *opposite* side chose to avoid the branch selected by their predecessors. Such strong consistency across the results suggests that the gradient, which is higher in the opposite branch (for example, see Fig. 6a, 100'), outperforms the contact-guidance in directing the trailing cells' migration. In other words, the majority of the followers try to avoid the branch with the preceding cells in it despite the wall they were initially in contact with. This is likely because they are trying to avoid a lower gradient created by the leading cells. Hence, the chemoattractant gradient effects *supersede* those of contact guidance, when asymmetries in the former are present.

Finally, **Supplementary Figure 4** shows that the NIH/3T3 results are in agreement with the NHDF trends presented in this

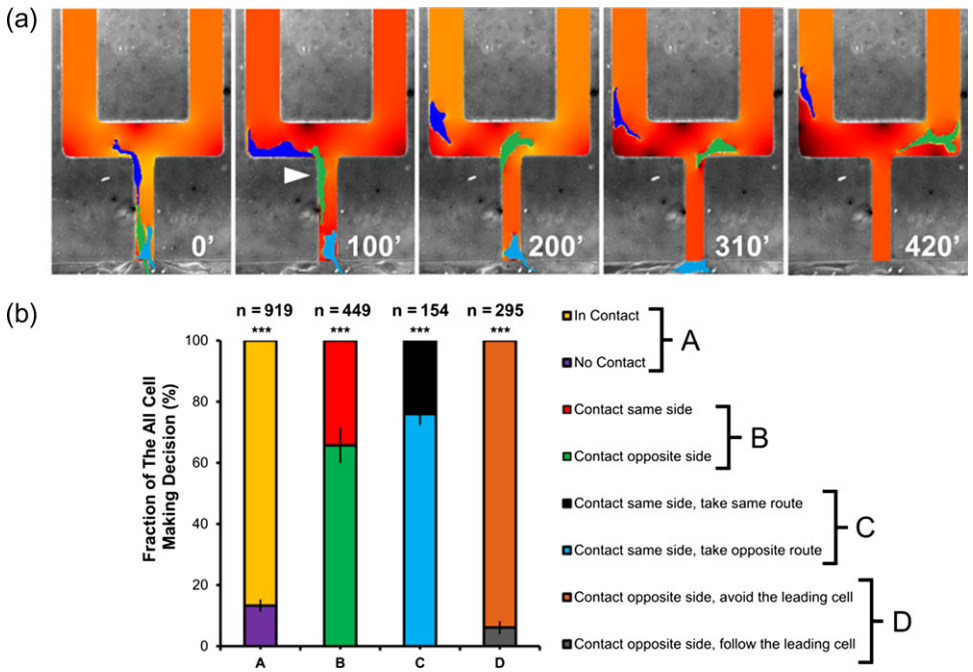

Figure 6. Contact guidance is superseded by chemoattractant gradient in the case of trailing NHDF cells (a) Montage showing the follower cells taking a path opposite to the wall that they contact due to the presence of the leading cells in the adjacent branch. White arrow indicates the second cell being in contact with the wall. Cells are false-colored to increase the visibility: blue is the leading, green is the follower and cyan is the 3rd. (b) Fraction of the follower cells making a directional decision. A: Fraction of follower cells contacting the feeder channel's wall; B: Fraction of the follower cells contacting the wall on the same side as the branch chosen by the leading cells versus those contacting the opposite wall; C: Fraction of the follower cells contacting the *same* side as the leading cells branch but taking the *opposite* route versus those taking the same route; D: Fraction of the follower cells contacting the *opposite* side but following the leading cells in its branch versus those contacting the *opposite* wall and avoiding the leading cell's branch. ***$p < 10^{-10}$.

section (with only a minor difference that the NIH/3T3 cells displayed less overall wall contact).

Mitosis increases the likelihood of daughters migrating into the narrower channels of width-asymmetric bifurcations

Finally, since the PDGF-BB is a fibroblasts 'mitoattractant' (i.e., both a chemoattractant [23–25] and a mitogen [26–29] at the same time), here we aim to provide a closer look at how cell divisions influence the fibroblast migratory decisions in the *width-asymmetric* bifurcations. First, we tracked the amount of divisions that occurred at different locations in the bifurcations. According to Fig. 7a, the extent of divisions varies between the different locations in the device. For example, most of them occurred at and near the bifurcation, because the PDGF-BB concentrations there begin to exceed the 5 ng/mL threshold at which the chemoattractant begins to act as a mitogen [27]. This result is also in agreement with our previous work in width-*symmetric* channels [18].

Furthermore, we observed that as the two daughters split up, they frequently move in opposite directions. This is also similar to the previous findings, where the daughters disregarded a global chemoattractant gradient and went against an oncoming traffic of undivided cells [18]. However, in the current width-*asymmetric* system, one of the daughters has a higher chance of migrating into the narrower branch (see Fig. 7b). This is in contrast to the undivided cells, which mostly avoid the narrower branches (see Fig. 7c). Hence, the cell division effects appear to dominate over the channel width cue. This finding is further supported by our NIH/3T3 results (see **Supplementary Figure 5**). Moreover, we did not observe any contact-guidance effects on the divided cells, suggesting that it too is inferior to mitosis.

DISCUSSION

Insights into cell migration in physically-confined environments are important for both understanding developmental biology in vivo and advancing artificial tissue growth strategies in vitro. Previous studies have demonstrated that there are multiple factors that contribute to the directional migration decisions of the cells inside micron-sized channels – analogous to physiological tissue pores – including channel width [9, 10, 17,

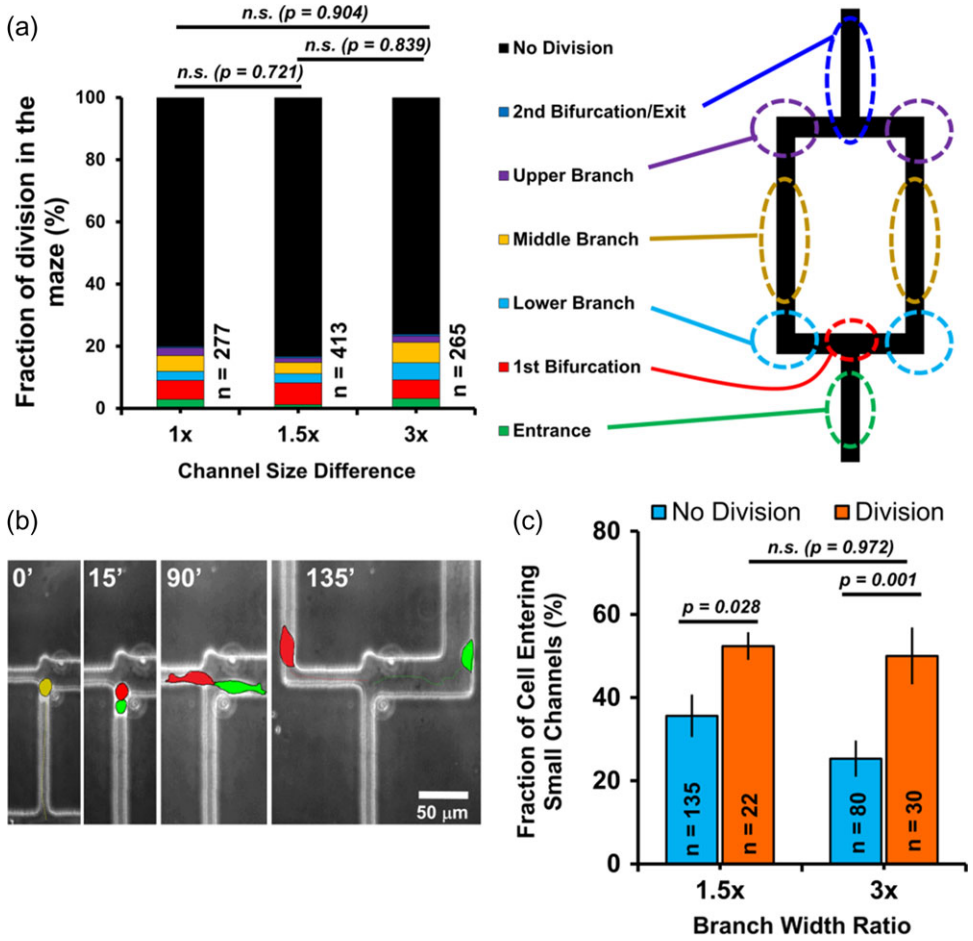

Figure 7. Divisions increase the chance of NHDF cells accessing the narrower branches in width-asymmetric bifurcations. (a) Spatial distribution of division occurrences within the device. (b) Phase contrast montage showing a daughter cell (red) migrating into the narrower branch. Cells are false-colored to improve visibility. Dashed lines indicate the tracked migration path (c) Bar graph showing that the fraction of the cells entering the narrower branches increases with divisions. The 'No Division' fraction is based on the number of cells entering the narrower branch relative to the total number of cells making decisions at the bifurcation (excluding those undergoing mitosis). The 'Division' fraction is based on the number of daughters entering the narrower branch relative to the total number of cells undergoing division in the device. The p-value between the mean of any two independent groups is found using the nonparametric Mann Whitney U test with a statistical significance level of 0.05; 'n' indicates the number of cells; 'n.s.': not statistically significant.

19, 40], chemical gradient [19], mitosis [13], and contact-guidance [10]. However, typically the effects of just one, or at most of two, such cues are explored at a time [20]. Yet, the cells encounter multiple simultaneous cues when navigating tissue pore environments in vivo. For that reason, our study examined how the four common cues compare relative to each other. Furthermore, it was performed with both human and mouse cells, in order to demonstrate the persistence of the observed patterns across different species.

Specifically, we were interested in the behavior of fibroblasts, which play a vital role in tissue formation: such as synthesizing, remodeling, and depositing extracellular matrix materials [14]. Although recently there have been several studies of fibroblast chemotaxis (especially migration in 3D collagen [41–44] and fibrin [43–45] matrices), to the best of our knowledge there have not been any reports comparing the relative importance of multiple migratory cues in guiding the cells' decision-making processes. For that reason, our study provides a first look at the comparison of the relative effects that the multiple directional cues have on the migration of individual fibroblast cells in tissue pore-mimicking confinement.

In order to do that, we created simple microfluidic bifurcations with two branches of different widths, and then induced fibroblast migration by establishing a global PDGF-BB gradient across these devices. We then used live phase contrast microscopy and manual data analysis in order to collect the statistics, which describe how the cells' decision making is affected by the visible cues. Additionally, we used a previously-developed image-based modeling methodology [18] in order to provide valuable insight into how localized gradient consumption by the cells affects their neighbors' directional decisions. Ultimately, we used the experimental and modeling results to perform a set of combinatorial comparisons, which then enabled us to rank the relative importance of the interrogated migratory cues.

Firstly, we found that a larger BWR between the two *asymmetric* bifurcated branches outdoes chemoattractant gradient differences in directing the fibroblasts. Specifically, the width asymmetry results in a large number of cells *following* each other into the wider branches. Similar preferences for the wider branches have also been shown in breast cancer cells by others [10]. Interestingly, the result is also in contradiction to our previous findings, which showed that the cells display sequence-dependent *alternation* between paths, when faced with a *symmetric* bifurcation [18]. Furthermore, given that the latter was found to be caused by changes in the chemoattractant concentration, the former can be concluded to be gradient-independent.

The mechanism behind the avoidance of the narrow branches can be attributed to the fact that migration into confined spaces requires that the cells expend additional energy: 1) the nucleus acts as a barrier due to its stiffness, so it takes extra effort to squeeze it through the narrow openings of the microfluidic channels [46, 47]; 2) the cytoskeletal architecture needs to become reorganized, such that its components are oriented along the axis of cell migration [48]; 3) the type and morphology of adhesions is modified, with α5-integrin, FAK, vinculin, and paxillin being dispersed along the body of the cell, instead of being localized at distinct sites (like in the absence of confinement) [48]; 4) gene expression and proliferation are altered via the action of mechanotransductive signaling pathways [48]. All of these energy expenditures make migrating into wider branches more favorable.

Secondly, we found that the cells commit to the wider branches *faster*, further signifying their preference for the less-constrained paths. The longer decision time was observed to be correlated with the cells searching for a more favorable choice, by extending their pseudopodia in the bifurcation branches. Such hesitation and extension of the protrusions in multiple directions have been reported by others [49]. However, when the wider branches became sufficiently crowded with the preceding cells, the follower cells still opted for the narrower branches. This, to the best of our knowledge, has not been demonstrated elsewhere.

Furthermore, we confirmed that these effects are indeed due to the width *asymmetry*, and not simply because of the availability of the wider channels. This was done by showing that the sequence-dependent alternation between the paths (which is expected from our prior work [18]) is retained in progressively wider *symmetric* (i.e., no difference between the available branch widths) bifurcations. Therefore, the localized chemoattractant concentration changes, created by the preceding cells, are predominant in guiding the following cells in the absence of the width asymmetry cue. This supports our earlier conclusion that the gradient effects are secondary to those of the width asymmetry.

Furthermore, in the absence of both the confinement and the gradient effects, the fibroblasts were found to be guided by the way that they contact the walls of the feeder channel. Contact guidance has been previously reported to depend on: the β1-Integrin (responsible for cellular binding to collagen type I), actomyosin contractility, and inhibition of the Cdc42 cell division control protein [10]. However, whether the chemical gradients have any impact on this behavior, and how the leading cells influence the trailing ones, have not yet been addressed. Therefore, our study has provided insight into these unknown questions.

Specifically, we found that in *symmetrical* gradient fields (i.e., inside bifurcations of identical branch widths and in the absence of any gradient changes by the leading cells), the contact guidance is dominant in regulating the cells' directional choices. Specifically, there is an 85% confidence that the cells will select the same path as the side that they contact. However, the contact-guidance loses importance when the PDGF-BB gradient is asymmetric, as the fibroblasts tend to follow the direction of the chemoattractant increase (regardless of which side they contact). This was demonstrated by showing that the follower fibroblasts avoid their predecessors, regardless of which wall that they are in contact with.

Lastly, from previous studies it is known that mitosis influences the direction of the migrating cells. Specifically, it was shown that daughter cells have a high chance of moving in *opposite* directions following cell division [13, 50]. However, these studies were conducted only in uniform concentration environments, which are not representative of the physiological cell migration. Consequently, our recent study [18] demonstrated that this effect remains true even when one of the daughters has to go against an established chemoattractant gradient (values of up to 1×10^{-3} mol/m^4 were investigated in this study). Finally, here we demonstrated that the mitosis induces the daughter cells to overcome their aversion for the more physically-constrained paths. Hence, it can be concluded that the mitosis is the strongest among the explored cues, given that the width asymmetry effects supersede those of the chemoattractant gradient and of the contact guidance. Furthermore, this result suggests that the divisions can circumvent the repelling nature of the constrained spaces in microscopic tissue pores and are therefore able to widely distribute the cells in a variety of spatial dimensions.

In order to explain why the daughter cells migrate opposite ways, as if they are blind to the other cues we hypothesize that the phenomenon can be attributed to differences in the relative

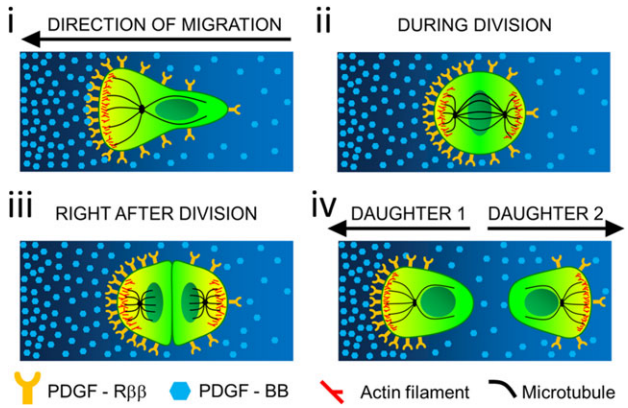

Figure 8. Proposed mechanism potentially explaining why daughter cells disregard migratory cues immediately after mitosis. i) A chemotaxing mother cell has an asymmetric distribution of PDGF-BB receptors over the surface of its membrane; ii & iii) As a result of mitosis, the daughter cells inherit PDGF-BB receptors only on the sides facing away from each other; iv) The two daughters migrate in opposite directions, as a result of the asymmetric receptor inheritance.

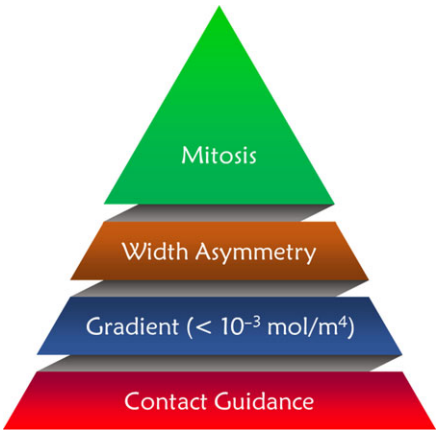

Figure 9. A hierarchical ranking of the observed relative importance that multiple migration cues have on directing single fibroblast migration in microscopic bifurcations. The chemoattractant gradient effects were tested up to a value of 1×10^{-3} mol/m^4.

expressions of chemoattractant receptors on their surfaces. For the specific case of the fibroblast PDGF-BB-driven chemotaxis, the chemoattractant membrane receptors plays a major role in mediating the migration process [26, 51]. Furthermore, the majority of the PDGF β-receptors are concentrated in caveolae [52, 53]; and these patches are distributed highly asymmetrically in migrating cells, due to their polarization [54, 55]. Similar asymmetric receptor distributions have been observed in other migrating cells before [56]. Therefore, it is possible that the daughter cells could inherit this asymmetry from the dividing mother (see Fig. 8). Hence, it would be interesting to image the PDGF-BB receptor distribution in the fibroblasts' membranes at the time of mitosis. However, immunofluorescent labeling of the PDGF receptors would also block the receptors sites, subsequently hindering the chemotaxis. Therefore, non-blocking fluorescent tags are needed in order to check this mechanism.

Furthermore, during mitosis the actin filaments, centrosomes, and other cellular components move to the opposite ends of the dividing mother's nucleus, and remain polarized [57–59]. This causes the two poles of the dividing mother cell to become the leading edges of each daughter cell (see Fig. 8). In particular, the actin-rich structures at one side of the daughter cells permit the formation of filopodia and lamellipodia in order to initiate directional movements [60]. As a result, the daughter cells are 'born' already polarized, with their leading edges pointing them in the directions away from each other [13]. Thus, this inherited bias in the organelle organization is also likely to contribute to their inability to change direction, and their subsequent disregard for other migratory cues.

In summary, from the findings presented above, we developed a pyramid hierarchy that ranks the relative importance of the different directional cues affecting the migration of fibroblasts (see Fig. 9). In this representation, the stronger the cue is, the higher its position is in the pyramid. A limitation of this work is that the pore sizes are much larger and the substrate (poly-D-lysine coated glass) is much stiffer in the maze compared to a typical extracellular matrix. Therefore, the results presented here are not a one-to-one comparison with the extracellular space of in vivo tissue. Nonetheless, they still carry practical implications for both understanding the biology of chemotactically driven morphogenesis processes in vivo as well as for artificial tissue design in vitro. For example, scaffold architectures could be optimized for achieving desired cell distributions by taking into account how the fibroblasts alternate the paths that they take at bifurcations. Thus, this study has potential widespread implications to the field of cell migration, as it provides an insight into the understanding of cellular behavior in the presence of complex combinations of different directional cues. It also opens a potential avenue to those who aim to control the cellular behavior (e.g., minimizing the product variability for the sake of successful biomanufacturing of artificial tissues).

CONCLUSION

In summary, we conducted a study ranking the relative importance that multiple migration cues have on directing single fibroblast migration in simple microfluidic bifurcations (meant to resemble the micro- constrainment of tissue pores in vivo). Specifically, chemoattractant concentration gradient, bifurcation branch width, mitosis and contact-guidance were among the investigated cues – each of which has been shown to affect cell migration individually. As a result of comparing them to each other, it was concluded that the fibroblasts prefer wider channels to narrower ones, even if the latter have more favorable chemoattractant conditions. In fact, the preference was so strong, that the cell sequence effects (i.e., alternating between paths) diminished relative to what has been observed in equal-width channels. The only exceptions to this occurred either when the wider branch became sufficiently crowded by the preceding cells, or when daughter cells were driven into the narrower branches by mitosis. Ultimately, we have come up with the following ranking of relative importance of the migration cues to directing fibroblast decisions: mitosis > wider channels > gradient > contact guidance. Finally, the presented results were confirmed to hold for both mouse and human fibroblasts. Therefore, they carry practical implications for developmental biology, multiple pathologies, and tissue engineering.

Supplementary data

Supplementary data is available at *INTBIO* online.

ACKNOWLEDGMENTS

The authors thank Gustavus and Louise Pfeiffer Research Foundation for their gracious funding of our work. Additionally, the authors would like to thank New Jersey Institute of Technology (NJIT)'s McNair Achievement and Provost Summer Research Programs, and Shodor's Blue Waters 2018-2019 Student Internship Program, for providing student labor for this project. NIH/3T3 and NHDF donations from Prof. Xiaoyang Xu's laboratory at NJIT's Department of Chemical and Materials Engineering and Dr. Duc-Huy Nguyen at Weill Cornell Medical College, respectively, are greatly appreciated. We would also like to thank Scott Baldwin at North Carolina State University for the invaluable discussions regarding fibroblast migration literature. Finally, we would also like to thank NJIT's Profs. Edward Dreyzin and Treena Arinzeh for pushing us beyond our limits.

Funding

This work was supported by the Gustavus and Louise Pfeiffer Research Foundation's Major Investment Grant, while the custom mask aligner was in part funded by NSF I-Corps Site Award [1450182].

Conflict of Interest

Authors Quang Long Pham, Anh Tong, Lydia N. Rodrigues, Yang Zhao, Migle Surblyte, Diomar Ramos, John Brito, Adwik Rahematpura, and Roman Voronov declare that they have no conflict of interest.

Ethical approval

This article does not contain any studies with human participants or animals performed by any of the authors.

References

1. Wong T, McGrath JA, Navsaria H. The role of fibroblasts in tissue engineering and regeneration. *Br J Dermatol* 2007;**156**:1149–55.
2. Sriram G, Bigliardi PL, Bigliardi-Qi M. Fibroblast heterogeneity and its implications for engineering organotypic skin models in vitro. *Eur J Cell Biol* 2015;**94**:483–512.
3. Kurosaka S, Kashina A. Cell biology of embryonic migration. *Birth Defects Res C Embryo Today* 2008;**84**:102–22.
4. Reig G, Pulgar E, Concha ML. Cell migration: from tissue culture to embryos. *Development* 2014;**141**:1999–2013.
5. Franz CM, Jones GE, Ridley AJ. Cell migration in development and disease. *Dev Cell* 2002;**2**:153–8.
6. Serbo JV, Kuo S, Lewis S et al. Patterning of Fibroblast and Matrix Anisotropy within 3D Confinement is Driven by the Cytoskeleton. *Adv Healthc Mater* 2016;**5**:146–58.
7. Alexander S, Koehl GE, Hirschberg M et al. Dynamic imaging of cancer growth and invasion: a modified skin-fold chamber model. *Histochem Cell Biol* 2008;**130**:1147–54.
8. Balzer EM, Tong Z, Paul CD et al. Physical confinement alters tumor cell adhesion and migration phenotypes. *FASEB J* 2012;**26**:4045–56.
9. Mak M, Erickson D. Mechanical decision trees for investigating and modulating single-cell cancer invasion dynamics. *Lab Chip* 2014;**14**:964–71.
10. Paul CD, Shea DJ, Mahoney MR et al. Interplay of the physical microenvironment, contact guidance, and intracellular signaling in cell decision making. *FASEB J* 2016;**30**:2161–70.
11. Wu D. Signaling mechanisms for regulation of chemotaxis. *Cell Res* 2005;**15**:52.
12. Haugh JM, Codazzi F, Teruel M et al. Spatial sensing in fibroblasts mediated by 3' phosphoinositides. *J Cell Biol* 2000;**151**:1269–80.
13. Albrecht-Buehler G. Daughter 3T3 cells. Are they mirror images of each other? *J Cell Biol* 1977;**72**:595–603.
14. Singer AJ, Clark RA. Cutaneous wound healing. *N Engl J Med* 1999;**341**:738–46.
15. Trepat X, Chen Z, Jacobson K. Cell migration. *Compr Physiol* 2012;**2**:2369–92.
16. Irimia D, Toner M. Spontaneous migration of cancer cells under conditions of mechanical confinement(). *Integr Biol* 2009;**1**:506–12.
17. Scherber C, Aranyosi AJ, Kulemann B et al. Epithelial cell guidance by self-generated EGF gradients. *Integr Biol* 2012;**4**:259–69.
18. Pham QL, Rodrigues LN, Maximov MA et al. Cell Sequence and Mitosis Affect Fibroblast Directional Decision-Making During Chemotaxis in Microfluidic Mazes. *Cell Mol Bioeng* 2018;**11**:483–94.
19. Ambravaneswaran V, Wong IY, Aranyosi AJ et al. Directional decisions during neutrophil chemotaxis inside bifurcating channels. *Integr Biol* 2010;**2**:639–47.
20. Lara Rodriguez L, Schneider IC. Directed cell migration in multi-cue environments. *Integr Biol* 2013;**5**:1306–23.
21. Melvin AT, Welf ES, Wang Y et al. In chemotaxing fibroblasts, both high-fidelity and weakly biased cell movements track the localization of PI3K signaling. *Biophys J* 2011;**100**:1893–901.
22. Schneider IC, Haugh JM. Quantitative elucidation of a distinct spatial gradient-sensing mechanism in fibroblasts. *J Cell Biol* 2005;**171**:883–92.
23. Seppä H, Grotendorst G, Seppä S et al. Platelet-derived growth factor in chemotactic for fibroblasts. *J Cell Biol* 1982;**92**:584–8.
24. Shreiber DI, Enever PA, Tranquillo RT. Effects of pdgf-bb on rat dermal fibroblast behavior in mechanically stressed and unstressed collagen and fibrin gels. *Exp Cell Res* 2001;**266**:155–66.
25. Siegbahn A, Hammacher A, Westermark B et al. Differential effects of the various isoforms of platelet-derived growth factor on chemotaxis of fibroblasts, monocytes, and granulocytes. *J Clin Invest* 1990;**85**:916–20.
26. Albini A, Adelmann-Grill BC, Muller PK. Fibroblast chemotaxis. *Coll Relat Res* 1985;**5**:283–96.
27. De Donatis A, Comito G, Buricchi F et al. Proliferation versus migration in platelet-derived growth factor signaling: the key role of endocytosis. *J Biol Chem* 2008;**283**:19948–56.
28. Lepisto J, Peltonen J, Vaha-Kreula M et al. Platelet-derived growth factor isoforms PDGF-AA, -AB and -BB exert specific effects on collagen gene expression and mitotic activity of cultured human wound fibroblasts. *Biochem Biophys Res Commun* 1995;**209**:393–9.
29. Lepisto J, Laato M, Niinikoski J et al. Effects of homodimeric isoforms of platelet-derived growth factor (PDGF-AA and PDGF-BB) on wound healing in rat. *J Surg Res* 1992;**53**:596–601.
30. Alam TA, Pham QL, Sikavitsas VI et al. Image-based modeling: A novel tool for realistic simulations of artificial bone cultures. *Technology* 2016;**04**:229–33.
31. Pham QL, Tong NAN, Mathew A et al. A compact low-cost low-maintenance open architecture mask aligner for fabrication of

multilayer microfluidics devices. *Biomicrofluidics* 2018;**12**: 044119.
32. Schneider CA, Rasband WS, Eliceiri KW. NIH Image to ImageJ: 25 years of image analysis. *Nat Methods* 2012;**9**:671–5.
33. Akar B, Jiang B, Somo SI et al. Biomaterials with persistent growth factor gradients in vivo accelerate vascularized tissue formation. *Biomaterials* 2015;**72**:61–73.
34. Menon SN, Flegg JA, McCue SW et al. Modelling the interaction of keratinocytes and fibroblasts during normal and abnormal wound healing processes. *Proc Biol Sci* 2012;**279**:3329–38.
35. Haugh JM. Deterministic model of dermal wound invasion incorporating receptor-mediated signal transduction and spatial gradient sensing. *Biophys J* 2006;**90**:2297–308.
36. Marx A, Backes C, Meese E et al. EDISON-WMW: exact dynamic programing solution of the Wilcoxon–Mann–Whitney test. *Genomics Proteomics Bioinform* 2016;**14**:55–61.
37. Zhang S, Charest PG, Firtel RA. Spatiotemporal regulation of Ras activity provides directional sensing. *Curr Biol* 2008;**18**: 1587–93.
38. Van Haastert PJ, Devreotes PN. Chemotaxis: signalling the way forward. *Nat Rev Mol Cell Biol* 2004;**5**:626.
39. Chodniewicz D, Klemke RL. Guiding cell migration through directed extension and stabilization of pseudopodia. *Exp Cell Res* 2004;**301**:31–7.
40. Rao S, Tata U, Lin V et al. The migration of cancer cells in gradually varying chemical gradients and mechanical constraints. *Micromachines* 2014;**5**:13.
41. Karamichos D, Lakshman N, Petroll WM. An experimental model for assessing fibroblast migration in 3-D collagen matrices. *Cell Motil Cytoskeleton* 2009;**66**:1–9.
42. Rhee S. Fibroblasts in three dimensional matrices: cell migration and matrix remodeling. *Exp Mol Med* 2009;**41**:858.
43. Miron-Mendoza M, Lin X, Ma L et al. Individual versus collective fibroblast spreading and migration: regulation by matrix composition in 3D culture. *Exp Eye Res* 2012;**99**:36–44.
44. Moreno-Arotzena O, Borau C, Movilla N et al. Fibroblast migration in 3D is controlled by haptotaxis in a non-muscle myosin II-dependent manner. *Ann Biomed Eng* 2015;**43**:3025–39.
45. King SJ, Asokan SB, Haynes EM et al. Lamellipodia are crucial for haptotactic sensing and response. *J Cell Sci* 2016;**129**: 2329–42.
46. McGregor AL, Hsia C-R, Lammerding J. Squish and squeeze—the nucleus as a physical barrier during migration in confined environments. *Curr Opin Cell Biol* 2016;**40**:32–40.
47. Davidson PM, Sliz J, Isermann P et al. Design of a microfluidic device to quantify dynamic intra-nuclear deformation during cell migration through confining environments. *Integr Biol* 2015;**7**:1534–46.
48. Paul CD, Hung W-C, Wirtz D et al. Engineered models of confined cell migration. *Annu Rev Biomed Eng* 2016;**18**:159–80.
49. Firtel RA, Chung CY. The molecular genetics of chemotaxis: sensing and responding to chemoattractant gradients. *Bioessays* 2000;**22**:603–15.
50. Albrecht-Buehler G. The phagokinetic tracks of 3T3 cells. *Cell* 1977;**11**:395–404.
51. Christensen ST, Veland IR, Schwab A et al. Analysis of primary cilia in directional cell migration in fibroblasts. *Methods Enzymol* 2013;**525**:45–58.
52. Moes MJ, Zhou Y, Boonstra J. Co-localization of the PDGF β-Receptor and Actin during PDGF Stimulation in Mouse Fibroblasts. *ISRN Cell Biol* 2012;**2012**:1–14. doi:10.5402/2012/568104.
53. Liu P, Ying Y, Ko Y-G et al. Localization of platelet-derived growth factor-stimulated phosphorylation cascade to caveolae. *J Biol Chem* 1996;**271**:10299–303.
54. Lentini D, Guzzi F, Pimpinelli F et al. Polarization of caveolins and caveolae during migration of immortalized neurons. *J Neurochem* 2008;**104**:514–23.
55. Parat M-O, Anand-Apte B, Fox PL. Differential caveolin-1 polarization in endothelial cells during migration in two and three dimensions. *Mol Biol Cell* 2003;**14**:3156–68.
56. Dona E, Barry JD, Valentin G et al. Directional tissue migration through a self-generated chemokine gradient. *Nature* 2013;**503**:285–9.
57. Kunda P, Baum B. The actin cytoskeleton in spindle assembly and positioning. *Trends Cell Biol* 2009;**19**:174–9.
58. Almonacid M, Terret M-É, Verlhac M-H. Actin-based spindle positioning: new insights from female gametes. *J Cell Sci* 2014;**127**:477–83.
59. Tang N, Marshall WF. Centrosome positioning in vertebrate development. *J Cell Sci* 2012;**125**:4951–61.
60. Mattila PK, Lappalainen P. Filopodia: molecular architecture and cellular functions. *Nat Rev Mol Cell Biol* 2008;**9**:446.